Applied Catalysis B: Environmental 257 (2019) 117909

Contents lists available at ScienceDirect

Applied Catalysis B: Environmental

journal homepage: www.elsevier.com/locate/apcatb

Mode of electrochemical deposition on the structure and morphology of bimetallic electrodes and its effect on nitrate reduction toward nitrogen selectivity

Jenn Fang Su[a], Wei-Fan Kuan[b], Huijuan Liu[c,d], C.P. Huang[a,*]

[a] Department of Civil and Environmental Engineering, University of Delaware, Newark, DE, 19716, USA
[b] Advanced Materials Characterization Laboratory, University of Delaware, Newark, DE, 19716, USA
[c] University of Chinese Academy of Sciences, Beijing, 100085, China
[d] Research Center for Eco-Environmental Sciences, Chinese Academy Sciences, Beijing, 100085, China

ARTICLE INFO

Keywords:
Nitrate reduction
Sn-Pd/SS electrode
Nitrogen selectivity
Electrodeposition
Bimetallic catalysts

ABSTRACT

This work investigates the effect of electrode preparation on nitrate reduction reaction with a focus on increasing nitrogen yield. Results indicated that stainless steel (SS) supported tin-palladium (SS/Sn-Pd) electrodes synthesized via multi-step electrodeposition at low voltage (< 10 V) substantially influenced the performance of nitrate transformation and nitrogen selectivity. Different electrodeposition programs, in terms of charging step and batch of metal solution, affected the crystallite size and surface morphology, i.e., roughness, and thus impacted nitrate reduction capability. Of the most significance, electrode prepared with one batch of solution containing both $SnCl_2$ and $PdCl_2$ at molar ratio of 4 to 1 exhibited the best performance in nearly 100% nitrate reduction and 81% nitrogen yield. The proposed low voltage electrochemical deposition process enables a new route to control the reactivity and selectivity of the reduction of oxyanions such as nitrate in water by manipulating electrode surface morphology.

1. Introduction

Lack of clean and safe water is a severe problem worldwide. Providing high quality water at sufficient quantity is a great challenge to humanity. One option for solving the shortage of quality water is reuse of used water. Unfortunately, conventional water treatment methods cannot achieve necessary efficiency, use too many chemicals, and consume too much energy. It has been reported that the water and wastewater industries consume 75 billion kWh of overall US annual energy demand [1]. Furthermore, the use of chemicals in conventional water purification plants creates unnecessary secondary pollution, which requires further treatment and additional cost.

Nitrate is one of the primary pollutants in water. Potentially, under certain ecological conditions, nitrate can be converted to nitrite and nitro-compounds (NOCs), which are health risk. For example, nitrate-derived nitrite in drinking water can cause methemoglobinemia, a main health risk associated with nitrate consumption [2]. Therefore, the US Environmental Protection Agency and World Health Organization have set a drinking water standard for nitrate at 50 mg/L [3].

Nitrate can be removed by the water using extractive methods such as adsorption, e.g., ion exchange resins [4] and separation/concentration, e.g., reverse osmosis [5] and electrodialysis [6]. The above methods are stable, effective, fast, easy to operate, and are appealing to small and medium-size treatment plants [7,8]. However, the above methods do not transform nitrate to benign species such as nitrogen molecule. Therefore, approaches such as biological denitrification [3,9], chemical [10–13], and electrochemical reduction [14–17] have been attempted to convert nitrate to other nitrogen species such as nitrogen and ammonia.

Biological denitrification using nitrate as electron acceptor, organic and inorganic substances as electron donor, and energy source for sustaining the microbial activities is a mature technology. The major advantage of the biological denitrification is the generation of relatively benign products. However, biological treatment of drinking water has limited application due to low public acceptance.

Chemical reduction process [10,11,13,18], such as zero-valence iron, Fe^0, converts nitrate to ammonium, NH_4^+, rapidly. Chemical reduction has many advantages, over method such as biological denitrification, including fast reaction rate and easy operation, but inevitable production of ammonia. Post-treatment for ammonium ion

* Corresponding author.
E-mail address: huang@udel.edu (C.P. Huang).

https://doi.org/10.1016/j.apcatb.2019.117909
Received 7 October 2018; Received in revised form 24 June 2019; Accepted 28 June 2019
Available online 29 June 2019
0926-3373/

removal by ion exchange resins or gas stripping is necessary to protect drinking water safety, which requires extra treatment costs.

Catalytic hydrogenation is another chemical reduction process in which hydrogen reduces nitrate over metallic catalysts. Furthermore, hydrogenation produces hydroxide ion, which may require further neutralization of the finished water [12]. Although catalytic hydrogenation can provide high nitrate reduction efficiency and possibly generate relatively benign nitrogen by-products, hydrogen has relatively low water solubility and concern of work place safety that limit its wide application for nitrate removal [19].

Electrochemical denitrification has become increasingly attractive in water treatment practices due to its environmental compatibility, work safety, reaction selectivity, robustness, and versatility. Applying an appropriate voltage on the working electrode enables electrochemical nitrate reduction. Under proper operation conditions, electrochemical process can minimize the production of secondary contaminants, and reduces process costs relative to biological denitrification and other chemical treatments. Studies have demonstrated that the electrochemical reduction of nitrate can take place over a wide variety of cathodic metals and alloys including Cu [20,21], Zn [22], Al [22], Pb [22], Rh [23], Cu-Ni [17], Cu-Zn [22], Cu-Sn [22], Cu-Pd [14,24–26], and Sn-Pd [27]. It appears that bimetallic catalysts, composed of a hydrogen-absorbing metal (e.g., Pd, Rh or Ru) [28,29] and an oxygen-absorbing metal (e.g., Cu or Sn) [30], generally exhibit superior performance than monometallic electrodes [31–34]. In the case of monometallic electrodes, adsorption of both oxygen and hydrogen atoms on the same metal decreased nitrate reduction rate [35]. Roué and co-workers studied the conversion of nitrate to nitrogen over Cu monometallic electrode [21] and $Cu_{0.7}Ni_{0.3}$ bimetallic electrode [17] and reported that the nitrogen yield over the $Cu_{0.7}Ni_{0.3}$ electrode was about two times that on the Cu electrode [17,21]. Other studies reported the nitrate reduction capability, in terms of N_2 yield, follow the decreasing order: $Pd_{0.62}Cu_{0.38}$ (76%) [36] > $Pd_{0.4}Cu_{0.6}$ (N_2 yield = 41%) [14] > Al (38.1%) [22] > $Sn_{0.85}Cu_{0.15}$ (34.4%) [22] > Pb (16%) [22] > Cu (9%) [22]. Generally bimetallic catalysts exhibit greater nitrogen selectivity than monometallic ones, except perhaps Al. The composition of bimetallic catalysts is one of the most important parameters controlling nitrogen selectivity.

Many factors can affect the nitrate reduction efficiency in terms of nitrogen selectivity. In addition to high surface area, rate of hydrogen and oxygen exchange reaction on the catalyst surface is also crucial to nitrogen selectivity. In essence, it is necessary to terminate the nitrate reduction reaction immediately by withholding the surface hydrogen atom rather than availing it to the surface nitrogen molecules, as soon as they appear, which tends to convert surface nitrogen molecules to ammonium.

Electrodeposition of metals on electrode supports in multiple steps has been shown to create smaller metal crystals and yield high surface area [37], which is known to promote adsorption of nitrate and increase catalytic response [38]. Therefore, the present research aimed at studying the mode of electrodeposition as a mean to enhance nitrate reduction toward high nitrogen selectivity. How the mode of electrochemical deposition affects the architecture of the catalysts? Can simple manipulation of the electrodeposition process of metallic catalysts achieve nitrogen selectivity? In order to answer the above questions, a Sn-Pd bimetallic catalyst was selected for this study, in which Sn was intended to be the O-affinity and Pd be the H-adsorbing metal, respectively. We first investigate the effects of multi-deposition process on electrode surface characteristics. Next, we explored the correlation between nitrogen yield and electrode surface property in order to establish much effective electrode preparation procedure. Finally, the nitrate reduction reaction pathway was proposed, based on steady-state approach, and the kinetics was analyzed.

2. Experimental

2.1. Materials

Sodium nitrate, of certified grade by American Chemical Society (ACS), was obtained from Fisher Scientific, Pittsburgh, PA, USA. Perchloric acid was purchased from ACROS, Fair Lawn, NJ, USA. Sodium hydroxide (purity > 97.0%) and Methanesulfonic acid were purchased from Sigma-Aldrich, St Luis, MO USA. The Mega-Pure System (MODEL MP-290) made deionized water. Platinum wire (Fisher Scientific, 1284987, od: 0.5 mm) was purchased from Fisher Scientific, Pittsburgh, PA, USA. Stainless steel mesh (corrosion-resistant 304 stainless steel woven wire cloth, 100 × 100 mesh, 0.0045″ wire diameter) was obtained from McMaster-Carr Co. Elmhurst, IL USA. Tin (II) chloride (purity > 98%), and palladium (II) chloride (purity > 98%) were purchased from Sigma-Aldrich, St Luis, MO USA.

2.2. Electrode preparation

The raw stainless-steel mesh was cut into pieces (ca. 1.5 cm × 8 cm) and washed with detergent thoroughly for surface cleaning. After cleaning, the mesh was rinsed with deionized water and dried in a dryer at room temperature for 1 h. The metal ion solutions were prepared by dissolving tin chloride ($SnCl_2$) and palladium chloride ($PdCl_2$) in deionized water at concentration of 0.1 M and 0.01 M, respectively. All electrodeposition experiments were carried out at room temperature by using a two-electrode system, which was connected to a potentiostat (Model WP705B, Vector-VID). Graphite was selected as the counter electrode. The washed stainless-steel mesh was the working electrode. Both electrodes were immersed in the metal ion solution in a 250-mL beaker. Metal deposition process was performed at constant total charge of 108 and 388.8 F for Pd and Sn, respectively, (Note: 1 F = 1A-sec) for all electrodes. During electrodeposition, the negative charge was delivered to the working electrode as to carry out the reduction of metal cations on the electrode surface. The total charge was delivered in several schemes, in terms of N, the number of individual solution tank used in the deposition process. Furthermore, in each tank of solution, the charge was applied in multiple steps, but the total charge remained constant at 108 and 388.8 F for Pd and Sn, respectively as mentioned above. For example, $N = 1$, both $SnCl_2$ and $PdCl_2$ were present in the same solution and deposition was carried out at −0.3 A @6 times (1.8 min per time for total 10.8 min) followed by −0.6 A @1 time for total 5.4 min. For N = 2, two separate $SnCl_2$ and $PdCl_2$ solutions were used. First, at −0.3 A@ 6 times (1.8 min per time, total 10.8 min) then −0.6 A @1 time (total 5.4 min) for Sn deposition, followed by −0.3 A @6 times (0.5 min per time, total 3 min) and −0.6 A @1 time (total 1.5 min) for Pd deposition. For N = 3, 3 different solutions. 1 $PdCl_2$, 1 $SnCl_2$ and then 1 $PdCl_2$ (i.e., first Pd, then Sn and finally Pd deposition) were used. Charge was applied at −0.3 A @ 6 times (0.25 min per time for total 1.5 min) and −0.6 A @ 1 time (0.75 min) for Pd deposition; then at −0.3 A @ 6 times (0.5 min per time for total 3 min) and −0.6 A @ 1 time (5.4 min) for Sn deposition; finally −0.3 A @6 times (0.25 min per time for total 1.5 min) and −0.6 A @ 1 time (0.75 min) for Pd deposition. Fig. 1 illustrates the details of metal deposition process, $N = 1$–14, respectively. In separate experiments, it was discovered that the nitrogen selectively was higher for electrodes with Pd being deposited last (data not shown). The overall composition of SS/Sn-Pd electrodes was fixed at [Sn]:[Pd] = 4:1 (SS/$Sn_{0.8}Pd_{0.2}$) for purpose of comparison.

Excess electrode precursor was rinsed numeral times with deionized water before the next deposition cycles. Finally, the resulted electrode, SS/Sn-Pd, was washed by deionized water and dried under ambient environment. The mole fraction, x_i, of the metal catalyst, i.e., Pd or Sn, on the electrode was determined by the following equation:

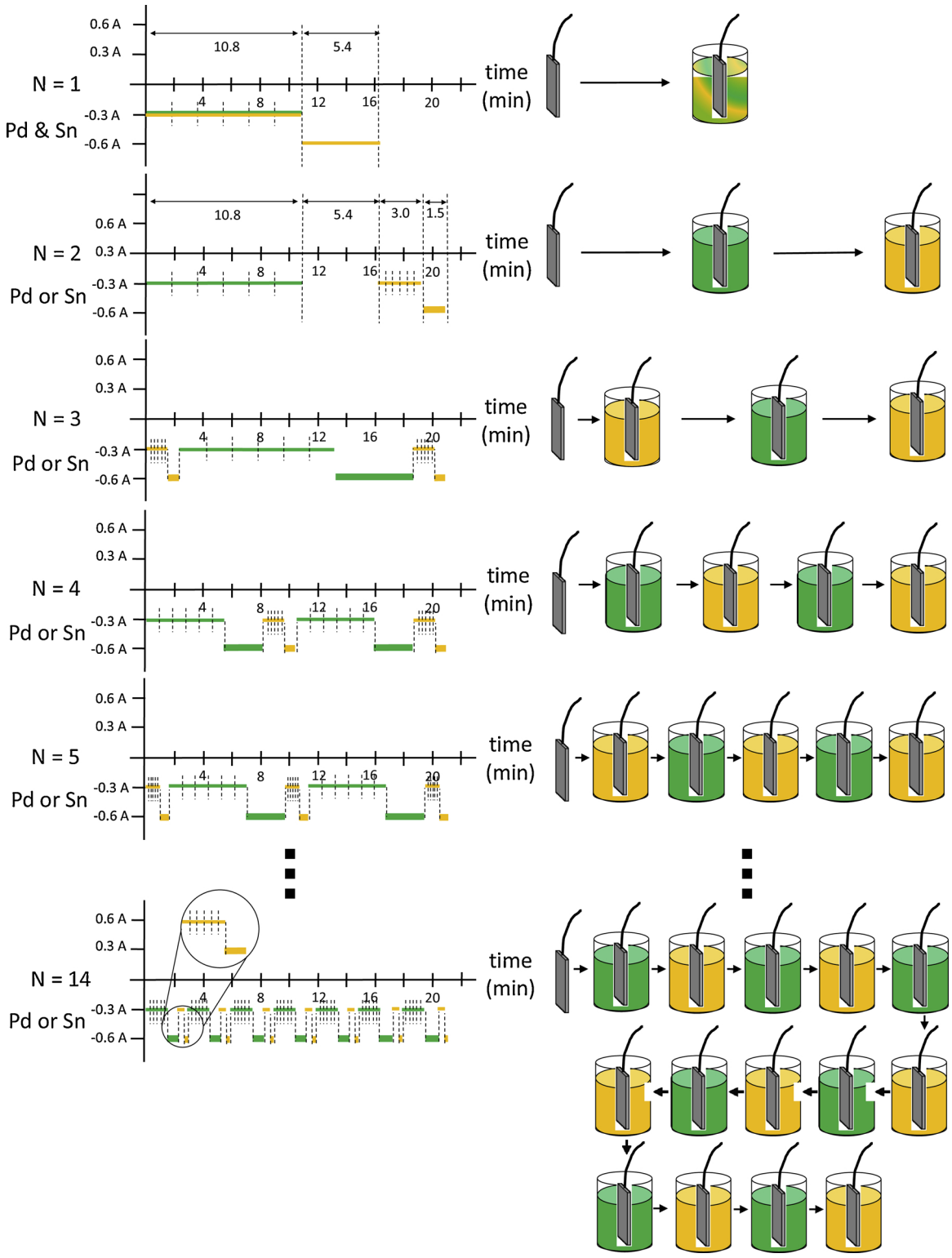

Fig. 1. Illustration of electrodeposition process on bimetallic catalysts in multiple steps. Y axis is current for electrodeposition and x axis is electrodeposition time. Green color represents $SnCl_2$ solution, and yellow color represents $PdCl_2$ solution. Each electrodeposition segment includes 6 times at −0.3 A + 1 time at −0.6 A. The overall composition and electrodeposition time for all electrodes were the same for comparison purpose (For interpretation of the references to colour in this figure legend, the reader is referred to the web version of this article).

$$x_i = \frac{(I_i \times t_i)/F}{\Sigma(I_i t_i)/F} = \frac{Q_i/F}{\sum Q_i/F} \quad (1)$$

where Q_i is the total electric charge consumed by the ith species (i.e., Sn or Pd) in coulombs, I_i and t_i are the current and the time involved in the deposition of the ith species, and F = 96,485 C/mol is the Faraday constant. The validity of Pd to Sn ratio was reasonably assured because the net charge for metal deposition was rightly adjustment by subtracting the same amount of charge dissipated to hydrogen production. In the current work, the composition of all synthesized electrodes were fixed at mole fraction of 0.8 Sn and 0.2 Pd, which is labeled as SS/

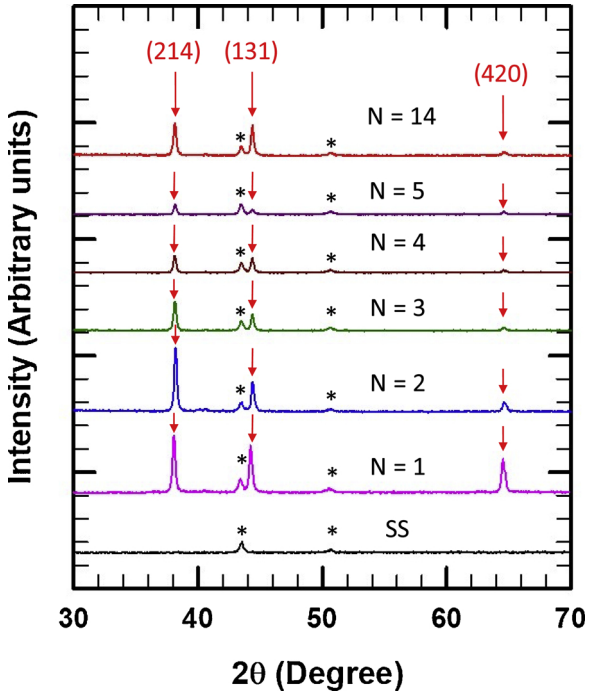

Fig. 2. XRD of SS/$Sn_{0.8}Pd_{0.2}$ with different *N* values, in which *N* is the total number of Sn deposition segments + Pd deposition segments. The overall composition of SS/$Sn_{0.8}Pd_{0.2}$ electrode was fixed at [Sn]:[Pd] = 4:1.

$Sn_{0.8}Pd_{0.2}$. Prior to each nitrate reduction experiment, the Sn-Pd electrode was regenerated by electrochemical reduction at constant current of 0.05 A for 1 min in a pure 0.1 M $HClO_4$ solution as to reduce the divalent tin and palladium ions to their elemental state [15]. In the absence of long-term durability tests, all nitrate reduction experiments were repeated 2–3 times using the same electrodes and results were highly reproducible.

2.3. Electrochemistry

All voltammetry experiments were carried out in a three-electrode system at room temperature. The three electrodes were connected to a potentiostat (model AFRDE 4, Pine Instrument Inc., USA), which controlled the applied voltage and measured responsive current. The stainless steel supported Sn, Sn-Pd, or Pd electrode was used as working electrodes. A platinum wire and a saturated calomel electrode (SCE) were used as countering electrode and reference electrode, respectively. The reaction vessel was a 500-mL beaker. The electrolyte was a 0.3 M $NaClO_4$ solution. Voltammetry experiments were operated at a sweep rate of 10 mV/s between −0.7 V to 0.3 V (vs. SCE) to evaluate the activity of the different electrodes for proton and nitrate reduction. In all cases, the voltammetric experiment was scanned 5 times in this potential range to achieve a relatively stable voltammogramm.

2.4. Analytical methods

The nitrate reduction experiments were performed in a two-electrode system with a graphite electrode as anode and the Sn-Pd electrode as cathode under 0.008 M $NaNO_3$ and constant current -0.04 A. Two compartment electrochemical cell was used as to assess the reactivity of the bimetallic electrodes under well controlled experimental conditions. An H-type reactor with a cationic membrane was used to keep low pH (pH = 1.5) in Cathodic compartment, while the reactor was being maintained under inert gas environment (argon-filled). The pH value remained relatively unchanged due to the presence of the strong acid in the electrolyzed solution. Nitrate, and nitrite were measured by a Dionex ion chromatograph (IC) system equipped with a GP50 pump, ED 40 conductance detector, Dionex IonPac AC20 column (4 mm × 250 mm.), and Dionex AS 40 automatic sampler. The effluent mobile phase with a flow rate of 1 mL/min was a mixture of dionized water and 50 mM NaOH, and the injection volume was 25 µL. At different intervals, 3 mL samples were withdrawn from the electrochemical cell for analysis. A Dionex ion chromatograph (IC) system equipped with a GP40 pump, CD 20 conductance detector, Dionex IonPac CS16 column (0.5 mm × 250 mm.), and Dionex AS 3500 automatic sampler was used to measure the ammonium. The effluent mobile phase with a flow rate of 1 mL/min was a mixture of dionized water and 0.1 M methanesulfonic acid, and the injection volume was 25 µL. Gaseous products from nitrate reduction reaction were determined by GC−MS with a HP 6890 series (Agilent Technologies, Santa Clara, USA) gas chromatograph equipped with a bonded polystyrene-divinylbenzene based column (HP-PLOT/Q, 15 m x 0.32 mm id). The mass spectrometric analysis was undertaken with a mass selective detector 5973 (Agilent Technologies, Santa Clara, USA). All nitrate reduction experiments were repeated 2 to 3 times using the same electrodes in order to confirm the electrode stability and the reproducibility of results.

The nitrogen yield (η), was defined by the following relationship:

$$\eta = \text{Conversion} \times \text{Selectivty} = \frac{\Delta C}{C_0} \times \frac{\Delta N}{\Delta C} \quad (2)$$

Where C_0, ΔC, ΔN, is the initial nitrate concentration, the change of nitrate concentration, and the change of molecular nitrogen concentration, respectively. Supporting Information S1 gives the detailed experiments for the optimization of electrodeposition programs.

2.5. Surface characterization of catalysts

Crystalline Sn-Pd alloy was identified by X-ray diffraction (XRD, Rigaku D-Max B) with Cu Kα radiation. Each sample was operated at 40 kV beam voltage and 40 mA current, and scanned from 30° to 70°. The elements and crystal structures were characterized by matching XRD pattern (JCPDS, PDF no. 85-1326) of each sample. Surface morphology and structure of the deposits were investigated by a scanning electron microscopy (JSM 7400F) at an accelerating voltage of 3 kV. Atomic force microscopy (AFM) measurements were carried out on a NanoIR-2 (Anasys Instruments), and the AFM images were captured using contact mode. The surface roughness was determined by averaging the measured values from six separated AFM scans on single Sn-Pd electrode.

3. Results and discussions

3.1. Surface characteristics as affected by the mode of metal deposition

Fig. 2 shows the XRD characteristics of SS/$Sn_{0.8}Pd_{0.2}$ electrodes prepared at different *N* values and deposition steps. In all cases, major diffraction peaks located at 2θ = 38.1, 44.4, and 64.6 (excluding SS peaks) were observed, indicating the presence of Sn_3Pd alloy with major crystal phases (214), (131), and (420), respectively [39]. XRD data in Fig. 2 showed relative peak intensity changes, which indicated changes in crystal facet distribution and potential complex formation between Sn and Pd metals among SS/$Sn_{0.8}Pd_{0.2}$ electrodes. The HRSEM images in Fig. 3 revealed clear influences by *N* and mode of metal electrodeposition on the surface morphologies. The electrode surface appeared to be composed of multiple nanoparticles at $N = 1$, $N = 2$ and $N = 14$; whereas the degree of surface roughness for electrodes with $N = 3$, 4, and 5 likely was relatively lower than that of $N = 1$. Fig. S6 shows the typical AFM image of electrode surface and Fig. S7 shows the relationship between surface roughness, ε (nm), and *N* value. Generally, results demonstrated a decrease in surface roughness (ε) with *N* increase from 1 to 5, then increase to a constant value around 150 nm at

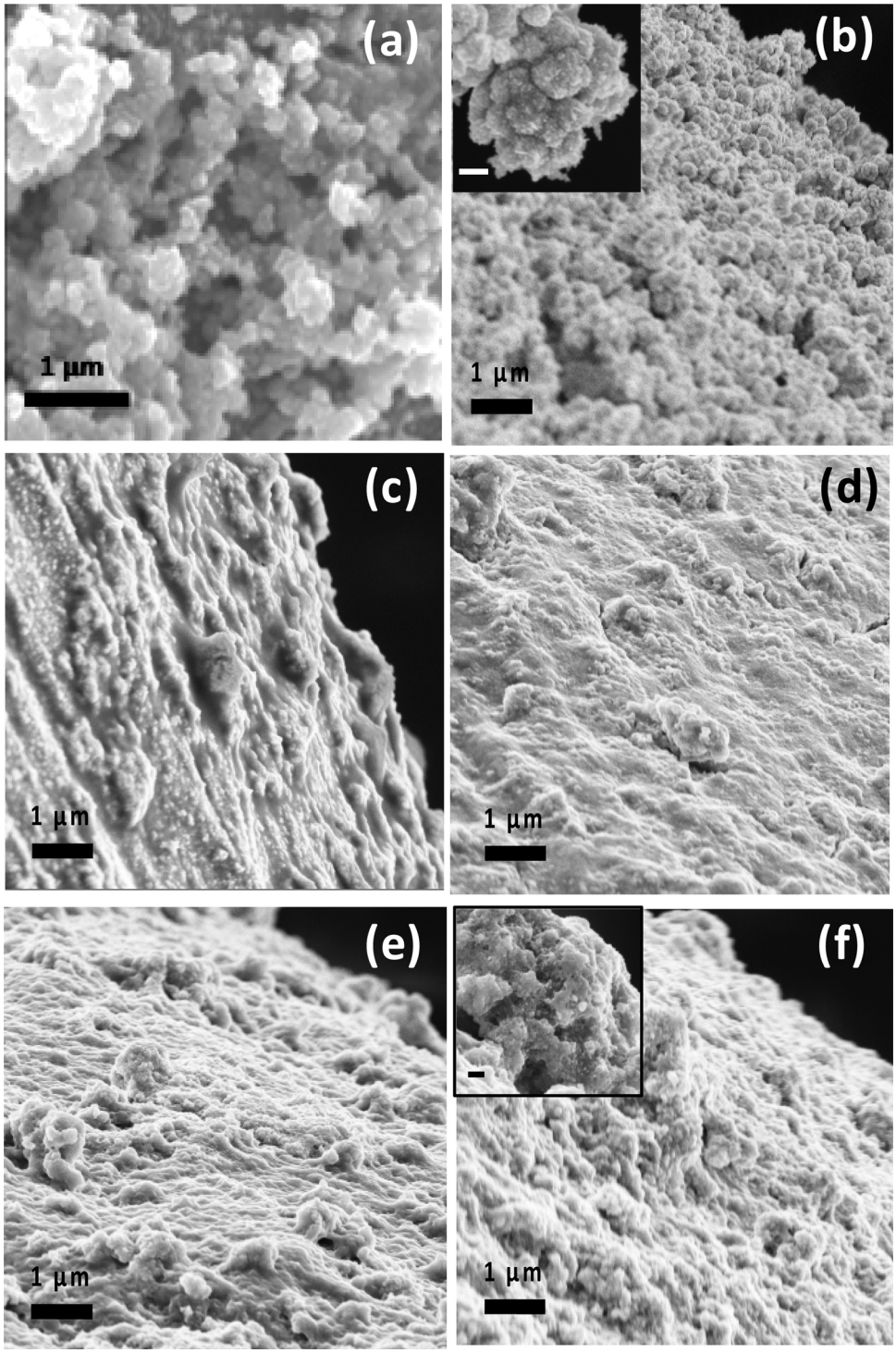

Fig. 3. HRSEM micrograph of SS/$Sn_{0.8}Pd_{0.2}$ electrodes at different *N* values, in which *N* is the total number of Sn deposition segments + Pd deposition segments. (a) $N = 1$; (b) $N = 2$; (c) $N = 3$; (d) $N = 4$; (e) $N = 5$; (f) $N = 14$. Scale bar in inset of (b) and (f) = 100 nm.

N > 6. The formation of metallic particles on the SS surface was a combination of several pertinent steps, including surface diffusion of metal ions, electron transfer converting the metal ions to elemental metallic particles, nucleation and coalescence of metal clusters [40]. Bordo and Rubahn studied the effect of deposition rate on structure and structure morphology of thin evaporated Al films on dielectrics and reported dependence of grain size on deposition rate [41]. Jeon et al. studied the effect of electro-deposition potential on the morphology and substrate of iron-based films on carbon steel substrate in alkaline solution and observed ion diffusion played a role on the grain sizes [42]. Our results showed that the surface became smooth as *N* increased from 1 to 5 due to formation of much dense clusters through the repeated dissolution and nucleation processes. At $N > 6$, the surface was occupied by clusters of nano-size metallic particles formed by the multiple charging steps that ultimately reached a steady-state in particle growth and attachment on the SS surface.

3.2. Nitrogen selectivity

Fig. 4 shows the change of pertinent nitrogen species during nitrate

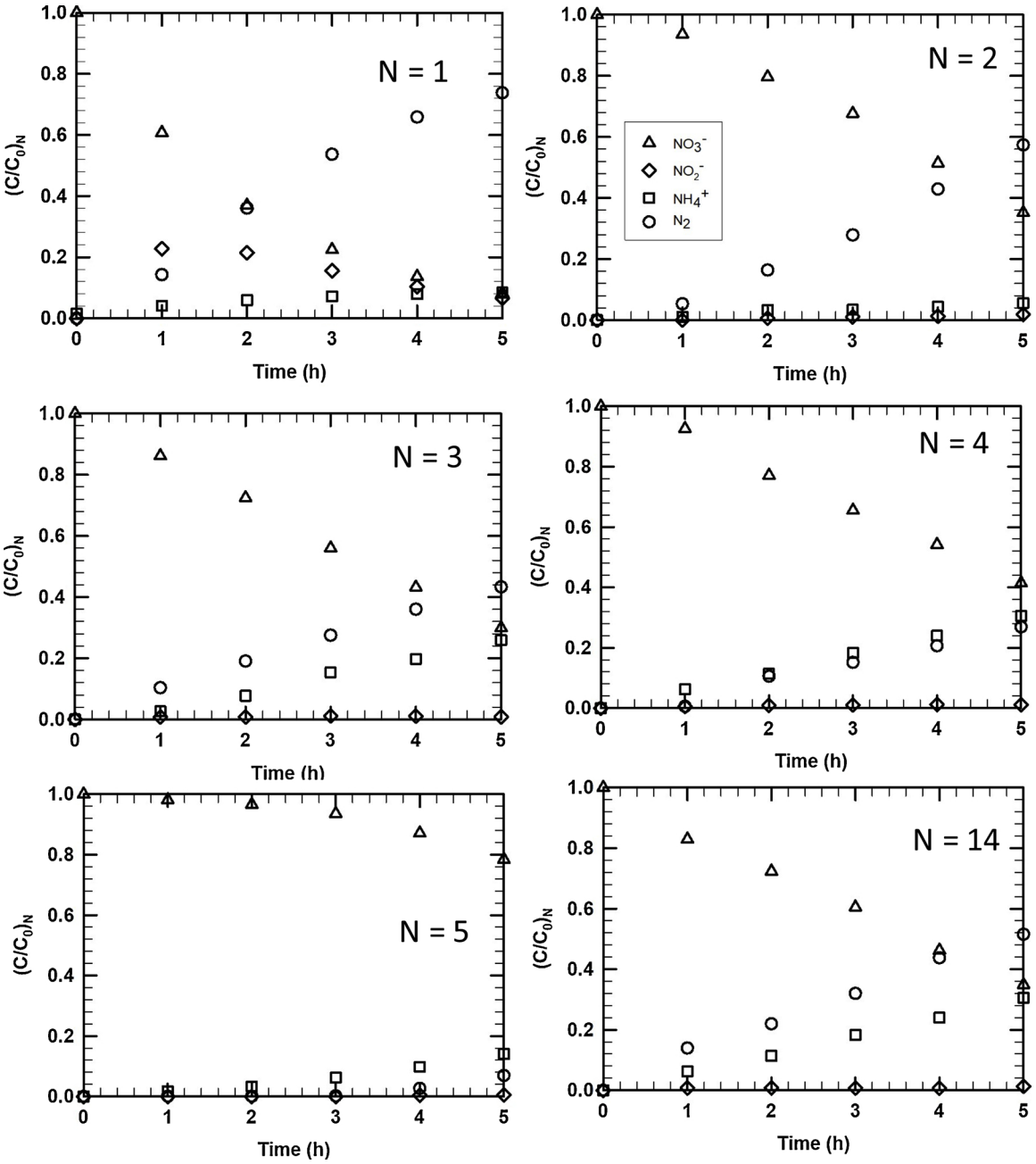

Fig. 4. Nitrate reduction reaction over SS/$Sn_{0.8}Pd_{0.2}$ at different mode of electrodeposition. Experimental conditions: [$HClO_4$] = 0.1 M, [$NaNO_3$] = 0.008 M, [DC current] = -0.04 A, Reaction time = 5 h, Temperature = 298 K.

reduction as a function of time over SS/$Sn_{0.8}Pd_{0.2}$ prepared at different *N,* e.g., 1–5, 14. Nitrate, nitrite, and ammonium were detected in the liquid phase while the gaseous nitrogen was detected and quantified by GC–MS and mass-balance. Note that the gaseous N_2O was not detected by GC–MS in all reactions. *Notably, the nitrate removal by electrode prepared in mixture solution containing both $SnCl_2$ and $PdCl_2$,* i.e., *SS/$Sn_{0.8}Pd_{0.2}$ (N = 1) was nearly 100% and the nitrogen yield reached about 81%.* Our nitrogen yield was relatively higher than most reported in the literature especially in electrochemical nitrate reduction, while ammonia yield remained relatively low at 14% (Table 1). Fig. 4 clearly shows the effect of the mode of deposition during electrode preparation on the reactivity and selectivity of nitrate reduction. For example, fraction of nitrogen generation decreased from 0.74 to mere 0.07 (or 74 to 7%) when *N* was increased from 1 to 5.

As mentioned in Section 3.1, variation in mode of electrodeposition likely led to changes in crystal facet distribution on SS/$Sn_{0.8}Pd_{0.2}$ electrodes, which might affect the nitrate reduction reaction. Koper et al. reported that nitrate reduction was a structure sensitive reaction [44]. They demonstrated that nitrate reduction was highly sensitive to the width of the Pt(100) terrace and N_2 formation was preferably occurred at the Pt(100) facet. As a result, N_2 formation ability decreased significantly when the (100) facets were perturbed by the (111) facets [44]. Kita et al. [45] and Feliu et al. [46] studied nitrate reduction over Pt single crystal electrode and reported that the reduction activity over Pt(100) was much greater than that on Pt(111) and Pt(110) facets [45,46]. Therefore, changes in crystal facet distribution induced by the mode of electrodeposition, are expected to influence nitrate reduction activity because of its structure sensitivity.

Three major crystal phases, i.e. Sn_3Pd(214), Sn_3Pd(131), and Sn_3Pd (420), were detected on the electrode surface of SS/$Sn_{0.8}Pd_{0.2}$ from

Table 1
Comparison of nitrogen selectivity by catalytic electrochemical nitrate reduction.

Cathode Material	Cathode Source	Cell Type	Experimental Conditions	Ammonia yield (%)	N_2 yield (%)	Ref.
Cu	Commercial	Single	pH = 12 0.1 M $NaNO_3$ 0.01 M NaOH 0.5 M NaCl I = 0.6 mA	26.4	30	[21]
Cu	Anodization	Divided	−1.5 V (vs. Ag/AgCl)	70	9	[22]
Zn	Commercial	Divided	−1.5 V (vs. Ag/AgCl)	46	N.A.	[22]
Al	Commercial	Divided	−1.8 V (vs. Ag/AgCl)	47	38.1	[22]
Pb	Commercial	Divided	−2.0 V (vs. Ag/AgCl)	64	16	[22]
$Cu_{0.6}Zn_{0.4}$	Commercial	Divided	−0.5 V (vs. Ag/AgCl)	75	2.08	[22]
$Sn_{0.85}Cu_{0.15}$	Commercial	Divided	−1.6 V (vs. Ag/AgCl)	2	7.6	[22]
$Sn_{0.85}Cu_{0.15}$	Commercial	Divided	−2.0 V (vs. Ag/AgCl)	40	34.4	[22]
$Pd_{0.4}Cu_{0.6}$	Electrodeposition	Single	pH = 7 50 ppm $NaNO_3$ −0.3 V (vs. SCE)	49	41	[14]
$Pd_{0.62}Cu_{0.38}$	Electrodeposition	Divided	0.1 M $NaNO_3$ 1 M NaOH −0.93 V (vs. SCE)	10	76	[36]
$Pd_{0.2}Sn_{0.8}$/SS (single deposition)	Electrodeposition	Divided	pH = 1.5 0.008 M $NaNO_3$ 0.1 M $HClO_4$ I = 0.04 A	24	34	This work
$Pd_{0.2}Sn_{0.8}$/SS (multiple deposition)	Electrodeposition	Divided	pH = 1.5 0.008 M $NaNO_3$ 0.1 M $HClO_4$ I = 0.04 A	6-28	10-60	This work
Blended $Sn_{0.8}Pd_{0.2}$/SS	Electrodeposition	Divided	pH = 1.5 0.008 M $NaNO_3$ 0.1 M $HClO_4$ I = 0.04 A	14	81	This work

XRD data. To investigate the influence of individual crystal phase on nitrate reduction, the apparent crystallite size, D, of each phase was calculated according to the Scherrer equation [47]:

$$D = \frac{K\lambda}{\beta\cos(2\theta/2)} \quad (3)$$

where K is the Scherrer constant, λ is the wavelength of the X-rays, 2θ is the diffraction angle, and β is the full width at half maximum of the selected peak. Table 2 shows the crystallite size of different phases, namely, Sn_3Pd(214), Sn_3Pd(131), and Sn_3Pd(420), resulted from different modes of electrodeposition. Fig. 5 gives the relationship between nitrogen yield and crystallite size. Smaller crystallite size was correlated closely to higher nitrogen yield in all phases. When nitrogen yield increased from 0.07 to 0.81, $D_{(214)}$ decreased from 2.53 nm to 1.98 nm, $D_{(131)}$ decreased from 3.95 nm to 2.52 nm, and $D_{(420)}$ decreased from 5.75 nm to 3.48 nm, respectively. Clearly, Sn_3Pd(420) exhibited the greatest drop in nitrogen yield, indicating Sn_3Pd(420) was the dominant phase compared to Sn_3Pd(214) and Sn_3Pd(131).

As the crystallite size variation is closely associated with crystal facet distribution [48], which potentially plays a role in modifying electrode surface roughness, further exploration on the relationship between nitrate reduction performance and surface roughness over the

Table 2
Crystallite size of Sn_3Pd(214), Sn_3Pd(131), and Sn_3Pd(420) at different mode of electrodeposition.

N	$D_{(214)}$ (nm)	$D_{(131)}$ (nm)	$D_{(420)}$ (nm)
1	1.98	2.52	3.48
2	2.23	2.62	4.37
3	2.34	2.57	5.64
4	2.53	2.72	5.88
5	2.53	3.95	5.75
14	2.34	2.44	4.89

N: the number of individual solution tank used in the deposition process.
$D_{(hkl)}$: crystallite size of phase (hkl).

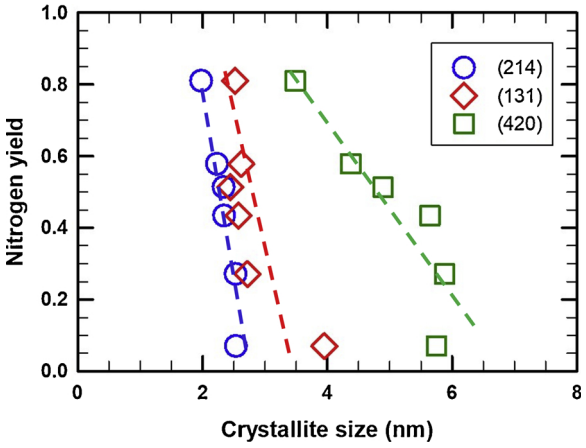

Fig. 5. Nitrogen yield as a function of crystallite size from Sn_3Pd(214), Sn_3Pd(131), and Sn_3Pd(420). Dash line is for eye guide.

SS/$Sn_{0.8}Pd_{0.2}$ electrodes were conducted. Fig. 6 reports the nitrogen yield as a function of electrode surface roughness, ε (nm). Interestingly, the nitrogen yield increased linearly with increase in surface roughness of electrodes. The result suggests clearly that increasing the roughness of electrode surface promotes the catalytic response of nitrate and nitrite reduction process due to the increase of surface area/adsorption sites, which is in agreement with other researchers [38,43]. Additionally, by the mode of electrodeposition, one can control the surface roughness of metallic electrodes such as our SS/$Sn_{0.8}Pd_{0.2}$ electrodes.

3.3. Rate of nitrogen reduction

Fig. 7(a) shows the CV curve of SS/Sn-Pd electrodes with Sn to Pd molar fraction of 1:0, 4:1, and 0:1, respectively, in the solution containing 0.3 M $HClO_4$. The CV curve was measured in the potential scanning from −0.7 V to 0.3 V (vs. SCE). A hydrogen ion adsorption

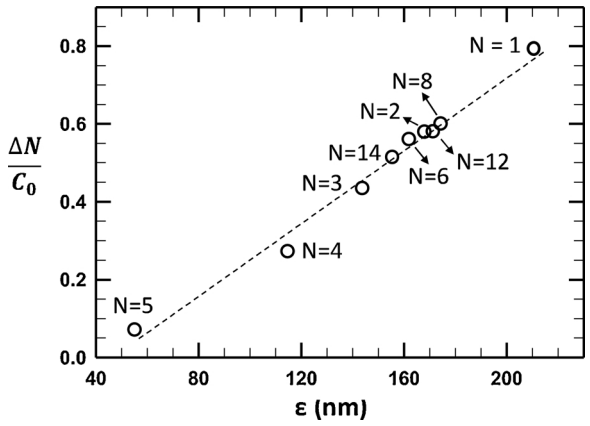

Fig. 6. Nitrogen yield as a function of surface roughness, ε, of electrodes. The data points are the average values of 6 separated AFM scan. Dash line is for eye guide.

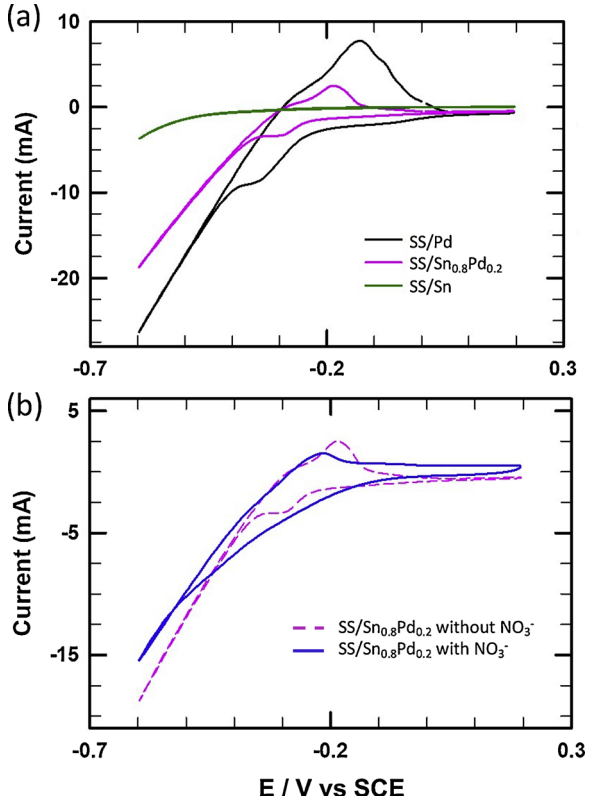

Fig. 7. (a) Cyclic voltammetric curve over SS/Pd, SS/$Sn_{0.8}Pd_{0.2}$, and SS/Sn electrode in 0.3 M $HClO_4$ solution. (b) Cyclic voltammetric curve over SS/$Sn_{0.8}Pd_{0.2}$ electrode in 0.008 M $NaNO_3$ and 0.3 M $HClO_4$ solution. Dash line is CV curve of SS/$Sn_{0.8}Pd_{0.2}$ electrode in the absence of $NaNO_3$ solution obtained from Fig. 7(a).

peak was observed during the cathodic sweep on all electrodes and there was a corresponding oxidation peak under anodic scans, suggesting the presence of reversible redox reaction [49]. Additionally, it was noted that the hydrogen ion adsorption peak decreased as the composition of Sn increased, indicating the blockage of adsorption sites from hydrogen atoms by Sn. Moreover, there was no hydrogen ion reduction and oxidation peaks occurred on the Sn/SS electrode, confirming the active role of Pd in the adsorption of H^+. Additionally, CV curve of SS/$Sn_{0.8}Pd_{0.2}$ in the solution containing 0.008 M $NaNO_3$ and 0.3 M $HClO_4$ is presented in Fig. 7(b). Comparing to CV curve of SS/$Sn_{0.8}Pd_{0.2}$ in the absence of nitrate ions (dash line), nitrate reduction over SS/$Sn_{0.8}Pd_{0.2}$ electrodes took place at the potential range from −0.2 V to −0.5 V.

According to above experimental results, the following reaction steps were proposed to describe nitrate reduction over the SS/$Sn_{0.8}Pd_{0.2}$ (e.g., $N = 1$) electrode. Note that the nitrate reduction in this work was carried out at constant current of −0.04 A and applied voltage in the range of 6 V–6.5 V. At the onset of the reaction, NO_3^- onto O-metal (i.e., Sn) [30] and H^+ adsorption on H-metal (i.e., Pd) [28,50] took place rapidly. In principle, H_2O will be adsorbed onto both Sn and Pd metals. However, since Pd has strong hydrogen absorption capacity than Sn, it is assumed that H_2O will prefer Pd to Sn sites.

$$NO_3^- + S_1 \leftrightarrows S_1NO_3^- \quad (4a)$$

$$H_2O + S_1 \leftrightarrows S_1H_2O \quad (4b)$$

$$H^+ + S_2 \leftrightarrows S_2H^+ \quad (4c)$$

$$H_2O + S_2 \leftrightarrows S_2H_2O \quad (4d)$$

Where S_1 is the vacant Sn surface site (O-metal) and S_2 is the vacant Pd surface site (H-metal) on the SS/Sn-Pd electrode. Direct electron attack (reduction) on surface protons and water molecules readily reduced proton and water molecules to hydrogens, S_2H.

$$S_2H^+ + e^- \rightarrow S_2H \quad (4e)$$

$$S_2H_2O + e^- \rightarrow S_2H + OH^- \quad (4f)$$

A series of reductions, commencing with surface NO_3^- and H atom, then occurred yielding various surface nitrogen species, such as $S_1NO_2^-$, S_1NO, S_1N_2O, S_1N_2, S_2NH, S_2NH_2, and S_2NH_3.

$$S_1NO_3^- + 2S_2H \rightarrow S_1NO_2^- + S_2H_2O \quad (4g)$$

$$S_1NO_2^- + S_2H \rightarrow S_1NO + S_2OH^- \quad (4h)$$

$$2S_1NO + 2S_2H \rightarrow S_1N_2O + S_2H_2O + S_1 + S_2 \quad (4i)$$

$$S_1N_2O + S_2H \rightarrow S_1N_2 + S_2OH \quad (4j)$$

$$S_1N_2 \rightarrow S_1 + N_2 \quad (4k)$$

$$S_1NO + S_2H \rightarrow S_2NH + S_1O \quad (4l)$$

$$S_2NH + S_2H \rightarrow S_2NH_2 + S_2 \quad (4m)$$

$$S_2NH_2 + S_2H \rightarrow S_2NH_3 + S_2 \quad (4n)$$

$$S_2NH_3 \rightarrow NH_3 + S_2 \quad (4o)$$

$$S_1NO_2^- \leftrightarrows S_1 + NO_2^- \quad (4p)$$

$$NH_3 + H_2O \leftrightarrows NH_4^+ + OH^- \quad (4q)$$

In summary, the main features of the above reaction scheme are: (1) adsorption of nitrate and water onto an empty Sn site via their oxygen atoms; (2) adsorption of hydrogen or water on the empty Pd site via their hydrogen atoms; (3) direct reduction of surface hydrogen atoms and water molecules on the Pd site; (4) indirect surface reduction of nitrate to nitrite. The indirect reduction mechanism was applied due to the non-linear nitrate conversion as a function of time shown in Fig. 4; (5) a series of surface reaction involved the surface hydrogen atoms (on the Pd site) with various surface oxy-nitrogen species (on the Sn site) eventually lead to the production of nitrogen molecules; (6) further reaction between the surface hydrogen species and surface oxy-nitrogen species (both on the Pd site) eventually yields ammonium ion. In this proposed mechanism, the main path for the desired nitrogen formation is from the reduction of nitrous oxide (N_2O), which is also reported in other literatures [51–57].

Based on the above reaction steps, the temporal concentration of major reaction products and nitrate can be derived as detailed in the Supporting Information S2 [14,58]. The temporal concentration of nitrate, nitrite, nitrogen gas, and ammonium are as the following.

$$C_{NO_3^-} = C^0_{NO_3^-} e^{-k_I t} \quad (5a)$$

$$C_{NO_2^-} = \frac{k_I C^0_{NO_3^-}}{k_{II} - k_I}(e^{-k_I t} - e^{-k_{II} t}) \quad (5b)$$

$$C_{N_2} = \frac{k_{III} C^0_{NO_3^-}}{k_{II} - k_I}(1 - e^{-k_I t}) + \frac{k_I k_{III} C^0_{NO_3^-}}{k_{II}(k_{II} - k_I)}(e^{-k_{II} t} - 1) \quad (5c)$$

$$C_{NH_4^+} = \frac{k_V C^0_{NO_3^-}}{k_{II} - k_I}(1 - e^{-k_I t}) + \frac{k_I k_V C^0_{NO_3^-}}{k_{II}(k_{II} - k_I)}(e^{-k_{II} t} - 1) \quad (5d)$$

where,

$$k_I = \frac{K_{4a} k_{4g} C_{S_1^0}}{K_{4b} C_{H_2O}} \quad (5e)$$

$$k_{II} = \frac{k_{4h} C_{S_1^0}(k_{4i} + k_{4l} C_{S_2^0})}{(k_{4i} + k_{4l}) K_{4p} K_{4b} C_{H_2O}} \quad (5f)$$

$$k_{III} = \frac{k_{4h} k_{4i} C_{S_1^0}}{(k_{4i} + k_{4l}) K_{4p} K_{4b} C_{H_2O}} \quad (5g)$$

$$k_V = \frac{k_{4h} k_{4l} C_{S_1^0} C_{S_2^0} K_{4q} C_{H^+}}{(k_{4i} + k_{4l}) K_{4p} K_{4b} C_{H_2O} C_{OH^-}} \quad (5h)$$

Eqs. (5a)–(5d) were fitted to the concentration data (nitrate, nitrite, nitrogen gas, and ammonium) in Fig. S8 (Note: the fitting results were shown in solid lines). The parametric rate constants, k_I, k_{II}, k_{III}, k_V were obtained using the minimal residuals method. The fitted kinetic constants were: k_I = 0.50 (h^{-1}), k_{II} = 1.08 (h^{-1}), k_{III} = 0.94 (h^{-1}), and k_V = 0.13 (h^{-1}). The agreement between the fitted and the experimental data shown in Fig. S8 confirmed the validity of the proposed mechanism of nitrate reduction.

3.4. Surface roughness and nitrogen selectivity

To rationalize the findings in Fig. 6, the nitrogen yield can be expressed in the following term:

$$\eta = \frac{\Delta C}{C_0} \times \frac{\Delta N}{\Delta C} = \frac{\Delta N}{C_0} = \frac{C_{N_2}}{C^0_{NO_3^-}} \quad (6a)$$

Where $C^o_{NO_3^-}$ and C_{N_2} are initial nitrate concentration and temporal nitrogen concentration, respectively. Combining Eqs. (4g)–(4j), one can simplify the nitrogen generation as the following:

$$S_1NO_3^- \xrightarrow{k_{N_2}} S_1N_2 \quad (6b)$$

and the reaction rate of nitrogen, R_{N_2} is:

$$R_{N_2} = \frac{dC_{N_2}}{dt} = k_{N_2} S_a \rho_c C_{S_1NO_3^-} \quad (6c)$$

in which k_{N_2} (m/h) is the reaction rate constant, S_a (m^2/g) and ρ_c (g/m^3) are specific surface area and density of the catalyst, respectively. The surface NO_3^- concentration, $C_{S_1NO_3^-}$, can be obtained by solving the following general equation of continuity [59]:

$$\frac{\partial C_{S_1NO_3^-}}{\partial t} + \frac{\partial}{\partial z}\left(-D_e \frac{\partial C_{S_1NO_3^-}}{\partial z}\right) - R_{S_1NO_3^-} = 0 \quad (6d)$$

where D_e (m^2/h) is the diffusion coefficient and $R_{S_1NO_3^-}$ is the reaction rate per unit volume of catalyst. Solving Eq. 6d and integrating Eq. 6c one has the concentration of nitrogen generation, C_{N_2}, which leads to the following nitrogen yield equation (detailed derivation in Supporting Information S3):

$$\eta = \frac{C_{N_2}}{C^0_{NO_3^-}} = t_{(t=5)} k_{N_2} S_a \rho_c \propto S_a \quad (6e)$$

According to Donoso et al. [60], the surface area is a linear relationship with surface roughness expressed in terms of R_{RMS}, supporting our unequivocally experimental data in Fig. 6 that nitrogen yield is a function of surface roughness.

In summary, our results show that electrodeposition procedure of bimetallic catalysts has strong significant influence on nitrate reduction and nitrogen yield. It is possible to enhance the catalyst efficiency, in terms of reactivity and selectivity, in a facile and low-voltage manner without changing the chemical composition and constituents. Our finding provides a promising and significant step forward in fabricating highly-efficient and cost-effective electrodes for future water treatment applications.

4. Conclusion

A novel design of bimetallic catalyst electrode for electrochemical nitrate reduction was proposed. This work demonstrates that at constant charge capacity, i.e., the product of electric current and depositing time, the mode of electrodeposition greatly affects the surface structural properties, including crystallite size and surface roughness, which govern the reduction of nitrate toward nitrogen selectivity. The total number of metal electrodeposition exhibits a significant impact on the crystallite size. Higher nitrogen yield is potentially correlated to smaller crystallite size, especially for crystal phase $Sn_3Pd(420)$. The surface roughness decreases with increase in the total number of metal solution batch, till 5 batches then increases as the solution batch increases then remain constant around 50–65% nitrogen yield. Most significantly, our work demonstrated that the $SS/Sn_{0.8}Pd_{0.2}$ electrode prepared from one single solution containing the Sn and Pd salts achieved nearly 100% nitrate removal and 81% nitrogen yield. Our $SS/Sn_{0.8}Pd_{0.2}$ electrode exhibited high nitrate reduction reactivity toward high nitrogen selectivity, which likely was resulted from the reduced crystallite size and enhanced surface roughness. More studies are needed to better understand the specific mechanism by which the mode of electrochemical deposition on the structure and surface morphology of catalytic electrodes. Equally important is how to control reactivity and selectivity by manipulating the structure and surface morphology. Overall, we have provided a different approach for the preparation of high-performing bimetallic catalyst electrode for the reduction of oxyanions such as nitrate. The methodology investigated will enable the design and synthesis of novel materials for applications in the remediation of impaired water.

Declarations of interest

None.

Acknowledgements

The materials presented in this paper were based upon work partially supported by National Science Foundation, Grant No. 0965984 under the Environmental Engineering Program, Division of Chemical, Bioengineering, Environmental, and Transport Systems. Additional support was provided by US NSF IOA grant no. 1632899.

Appendix A. Supplementary data

Supplementary material related to this article can be found, in the online version, at doi:https://doi.org/10.1016/j.apcatb.2019.117909.

References

[1] F.R. Spellman, Water & Wastewater Infrastructure: Energy Efficiency and Sustainability, CRC Press, 2013 463 pp.
[2] D.M. Manassaram, L.C. Backer, D.M. Moll, A review of nitrates in drinking water: maternal exposure and adverse reproductive and developmental outcomes, Environ. Health Perspect. 114 (2006) 320–327.
[3] J. Wang, L. Chu, Biological nitrate removal from water and wastewater by solid-

phase denitrification process, Biotechnol. Adv. 34 (2016) 1103–1112.
[4] B.U. Bae, Y.H. Jung, W.W. Han, H.S. Shin, Improved brine recycling during nitrate removal using ion exchange, Water Res. 36 (2006) 3330–3340.
[5] J.J. Schoeman, A. Steyn, Nitrate removal with reverse osmosis in a rural area in South Africa, Desalination 155 (2003) 15–26.
[6] L.J. Banasiak, A.I. Schäfer, Removal of boron, fluoride and nitrate by electrodialysis in the presence of organic matter, J. Membr. Sci. 334 (2009) 101–109.
[7] A. Kapoor, T. Viraraghavan, Nitrate removal from drinking water—review, J. Environ. Eng. 123 (1997) 371–380.
[8] G.K. Luk, W.C. Au-Yeung, Experimental investigation on the chemical reduction of nitrate from groundwater, Adv. Environ. Res. 6 (2002) 441–453.
[9] A. Bhatnagar, M. Sillanpää, A review of emerging adsorbents for nitrate removal from water, Chem. Eng. J. 168 (2011) 493–504.
[10] C. Della Rocca, V. Belgiorno, S. Meriç, Overview of in-situ applicable nitrate removal processes, Desalination 204 (2007) 46–62.
[11] X. Fan, X. Guan, J. Ma, H. Ai, Kinetics and corrosion products of aqueous nitrate reduction by iron powder without reaction conditions control, J. Environ. Sci. 21 (2009) 1028–1035.
[12] J.C. Fanning, The chemical reduction of nitrate in aqueous solution, Coord. Chem. Rev. 199 (2000) 159–179.
[13] C.P. Huang, H.W. Wang, P.C. Chiu, Nitrate reduction by metallic iron, Water Res. 32 (1998) 2257–2264.
[14] J.F. Su, I. Ruzybayev, I. Shah, C.P. Huang, The electrochemical reduction of nitrate over micro-architectured metal electrodes with stainless steel scaffold, Appl. Catal. B 180 (2016) 199–209.
[15] M. Motahar Hossain, K. Nakata, T. Kawaguchi, K. Shimazu, Reduction of nitrate on electrochemically pre-reduced tin-modified palladium electrodes, J. Electroanal. Chem. 707 (2013) 59–65.
[16] I. Katsounaros, D. Ipsakis, C. Polatides, G. Kyriacou, Efficient electrochemical reduction of nitrate to nitrogen on tin cathode at very high cathodic potentials, Electrochim. Acta 52 (2006) 1329–1338.
[17] D. Reyter, D. Bélanger, L. Roué, Optimization of the cathode material for nitrate removal by a paired electrolysis process, J. Hazard. Mater. 192 (2011) 507–513.
[18] J.M. Rodríguez-Maroto, F. García-Herruzo, A. García-Rubio, C. Gómez-Lahoz, C. Vereda-Alonso, Kinetics of the chemical reduction of nitrate by zero-valent iron, Chemosphere 74 (2009) 804–809.
[19] Y. Yun, Z. Li, Y.H. Chen, M. Saino, S. Cheng, L. Zheng, Reduction of nitrate in secondary effluent of wastewater treatment plants by Fe^0 reductant and Pd–Cu/graphene catalyst, Water Air Soil Pollut. 227 (2016) 111–10.
[20] C. Polatides, G. Kyriacou, Electrochemical reduction of nitrate ion on various cathodes – reaction kinetics on bronze cathode, J. Appl. Electrochem. 35 (2005) 421–427.
[21] D. Reyter, D. Bélanger, L. Roué, Nitrate removal by a paired electrolysis on copper and Ti/IrO_2 coupled electrodes – influence of the anode/cathode surface area ratio, Water Res. 44 (2010) 1918–1926.
[22] C. Polatides, G. Kyriacou, Electrochemical reduction of nitrate ion on various cathodes - reaction kinetics on bronze cathode, J. Appl. Electrochem. 35 (2005) 421–427.
[23] I. Katsounaros, M. Dortsiou, C. Polatides, S. Preston, T. Kypraios, G. Kyriacou, Reaction pathways in the electrochemical reduction of nitrate on tin, Electrochim. Acta 71 (2012) 270–276.
[24] L. Lemaignen, C. Tong, V. Begon, R. Burch, D. Chadwick, Catalytic denitrification of water with palladium-based catalysts supported on activated carbons, Environ. Catal.: A Step Forward 75 (2002) 43–48.
[25] A.C.A. de Vooys, R.A. van Santen, J.A.R. van Veen, Electrocatalytic reduction of NO_3^- on palladium/copper electrodes, J. Mol. Catal. A Chem. 154 (2000) 203–215.
[26] D. Reyter, D. Bélanger, L. Roué, Elaboration of Cu − Pd films by coelectrodeposition: application to nitrate electroreduction, J. Phys. Chem. C. 113 (2009) 290–297.
[27] K. Shimazu, R. Goto, S. Piao, R. Kayama, K. Nakata, Y. Yoshinaga, Reduction of nitrate ions on tin-modified palladium thin film electrodes, J. Electroanal. Chem. 601 (2007) 161–168.
[28] L. Zaluski, A. Zaluska, P. Tessier, J.O. Ström-Olsen, R. Schulz, Catalytic effect of Pd on hydrogen absorption in mechanically alloyed Mg_2Ni, $LaNi_5$ and FeTi, J. Alloys Compd. 217 (1995) 295–300.
[29] T. Tanaka, D.E. Azofeifa, Theory of hydrogen absorption in metal hydrides, in: C.B. Satterthwaite, P. Jenna (Eds.), Electronic Structure and Properties of Hydrogen in Metals, Springer US, Boston, MA, 1983, pp. 79–84.
[30] R.H. Thurston, The Materials of Engineering, John Wiley & Sons, New York, NY, 1984.
[31] O.S.G.P. Soares, J.J.M. Órfão, M.F.R. Pereira, Nitrate reduction with hydrogen in the presence of physical mixtures with mono and bimetallic catalysts and ions in solution, Appl. Catal. B: Environ. 102 (2011) 424–432.
[32] F. Epron, F. Gauthard, C. Pinéda, J. Barbier, Catalytic reduction of nitrate and nitrite on Pt–Cu/Al_2O_3 catalysts in aqueous solution: role of the interaction between copper and platinum in the reaction, J. Catal. 198 (2001) 309–318.
[33] L. Mattarozzi, S. Cattarin, N. Comisso, P. Guerriero, M. Musiani, L. Vázquez-Gómez, Electrochemical reduction of nitrate and nitrite in alkaline media at CuNi alloy electrodes, Electrochim. Acta 89 (2013) 488–496.
[34] L. Mattarozzi, S. Cattarin, N. Comisso, R. Gerbasi, P. Guerriero, M. Musiani, E. Verlato, Electrodeposition of compact and porous Cu-Pd alloy layers and their application to nitrate reduction in alkali, Electrochim. Acta 230 (2017) 365–372.
[35] J. Batista, A. Pintar, M. Ceh, Characterization of supported Pd-Cu bimetallic catalysts by SEM, EDXS, AES and catalytic selectivity measurements, Catal. Letters 43 (1997) 79–84.
[36] D. Reyter, D. Bélanger, L. Roué, Elaboration of Cu − Pd films by coelectrodeposition: application to nitrate electroreduction, J. Phys. Chem. C 113 (2009) 290–297.
[37] R.M. Penner, Mesoscopic metal particles and wires by electrodeposition, J. Phys. Chem. B 106 (2002) 3339–3353.
[38] M. Li, C. Feng, Z. Zhang, S. Yang, N. Sugiura, Treatment of nitrate contaminated water using an electrochemical method, Bioresour. Technol. 101 (2010) 6553–6557.
[39] O.T. Woo, J. Rezek, M. Schlesinger, X-ray diffraction analyses of liquid-phase sintered compounds of Pd3Sn and Ni3Sn, Mater. Sci. Eng. 18 (1975) 163–165.
[40] D.L. Smith, Thin Film Deposition: Principles and Practice, McGraw-Hill, Inc., New York, 1995 616 pp.
[41] K. Bordo, H.G. Rubahn, Effect of deposition rae structure and surface morphology of thin evaporated Al film on dielectric and semiconductors, Mater. Sci. 18 (2012) 313–317.
[42] S.H. Jeon, G.D. Song, D.H. Hur, Effects of deposition potentials on the morphology and structure of iron-based films on carbon steel substrate in an alkaline solution, Adv. Mater. Sci. Eng. 2016 (2016) 90384789 pp.
[43] I.G. Casella, M. Gatta, Electrochemical reduction of NO^{3-} and NO^{2-} on a composite copper thallium electrode in alkaline solutions, J. Electroanal. Chem. 568 (2004) 183–188.
[44] A.S. Bandarenka, M.T.M. Koper, Structural and electronic effects in heterogeneous electrocatalysis: toward a rational design of electrocatalysts, J. Catal. 308 (2013) 11–24.
[45] M.C. Figueiredo, J. Solla-Gullón, F.J. Vidal-Iglesias, V. Climent, J.M. Feliu, Nitrate reduction at Pt(1 0 0) single crystals and preferentially oriented nanoparticles in neutral media, Catal. Today 202 (2013) 2–11.
[46] S. Ye, H. Hattori, H. Kati, Reduction of nitrite and NO on platinum single-crystal electrode in alkaline solution, Ber. Bunsen-Ges. Phys. Chem. 96 (1992) 1884–1886.
[47] A.L. Patterson, The Scherrer formula for X-ray particle size determination, Phys. Rev. 56 (1939) 978.
[48] S.S. John, I. Dutta, A.P. Angelopoulos, Synthesis and characterization of electrocatalytically active Platinum atom clusters and monodisperse single crystals, J. Phys. Chem. C 114 (2010) 13515–13525.
[49] I. Ávila-García, M. Plata-Torres, M.A. Domínguez-Crespo, C. Ramírez-Rodríguez, E.M. Arce-Estrada, Electrochemical study of Pt–Pd, Pt–Ru, Pt–Rh and Pt–Sn/C in acid media for hydrogen adsorption–desorption reaction, J. Alloys Compd. 434–435 (2007) 764–767.
[50] C.B. Satterthwaite, P. Jena (Eds.), Electronic Structure and Properties of Hydrogen in Metals, Springer US, Boston, MA, 1983.
[51] A.C.A. de Vooys, M.T.M. Koper, R.A. van Santen, J.A.R. van Veen, Mechanistic study on the electrocatalytic reduction of nitric oxide on transition-metal electrodes, J. Catal. 202 (2001) 387–394.
[52] J. Souza-Garcia, E.A. Ticianelli, V. Climent, J.M. Feliu, Nitrate reduction on Pt single crystals with Pd multilayer, Electrochim. Acta 54 (2009) 2094–2101.
[53] F.R. Rima, K. Nakata, K. Shimazu, M. Osawa, Surface enhanced infrared absorption spectroscopic studies of adsorbed nitrate, nitric oxide, and related compounds. 3. Formation and reduction of adsorbed nitrite at a platinum electrode, J. Phys. Chem. C 114 (2010) 6011–6018.
[54] M. Duca, B. van der Klugt, M.T.M. Koper, Electrocatalytic reduction of nitrite on transition and coinage metals, Electrochim. Acta 68 (2012) 32–43.
[55] G.E. Dima, A.C.A. de Vooys, M.T.M. Koper, Electrocatalytic reduction of nitrate at low concentration on coinage and transition-metal electrodes in acid solutions, J. Electroanal. Chem. 554 (2003) 15–23.
[56] M. Duca, M.T.M. Koper, Powering denitrification: the perspectives of electrocatalytic nitrate reduction, Energy Environ. Sci. 5 (2012) 9726–9742.
[57] V. Rosca, M. Duca, M.T. de Groot, M.T.M. Koper, Nitrogen cycle electrocatalysis, Chem. Rev. 109 (2009) (2012) 2209–2244.
[58] O.S.G.P. Soares, X. Fan, J.J.M. Órfão, A.A. Lapkin, M.F.R. Pereira, Kinetic modeling of nitrate reduction catalyzed by Pd–Cu supported on carbon nanotubes, Ind. Eng. Chem. Res. 51 (2012) 4854–4860.
[59] H.S. Fogler, Elements of Chemical Reaction Engineering, Prentice Hall, N.J, 1999 957 pp.
[60] M.G. Donoso, A. Méndez-Vilas, J.M. Bruque, M.L. González-Martin, On the relationship between common amplitude surface roughness parameters and surface area: implications for the study of cell–material interactions, 1st International Conference on Environmental, Industrial and Applied Microbiology 59 (2007) 245–251.